


Phonon-induced modification of quantum criticality

Abhisek Samanta,^{1,*} Efrat Shimshoni,^{2,†} and Daniel Podolsky^{1,‡}

¹Physics Department, Technion, Haifa 32000, Israel

²Department of Physics, Bar-Ilan University, Ramat Gan 52900, Israel

 (Received 29 April 2022; accepted 21 July 2022; published 29 July 2022)

We study the effect of acoustic phonons on the quantum phase transition in the $O(N)$ model. We develop a renormalization group (RG) analysis near $(3+1)$ space-time dimensions and derive the RG equations using an ϵ expansion. Our results indicate that when the number of flavors of the underlying $O(N)$ model exceeds a critical number $N_c = 4$, the quantum transition remains second-order of the Wilson-Fisher type while, for $N \leq 4$, it is a weakly first-order transition. We characterize this weakly first-order transition by a length scale ξ^* , below which the behavior appears to be critical. At finite temperatures for $N \leq 4$, a tricritical point separates the weakly first-order and second-order transitions.

DOI: [10.1103/PhysRevB.106.035154](https://doi.org/10.1103/PhysRevB.106.035154)

I. INTRODUCTION

The fate of the second-order quantum phase transition in the presence of lattice vibrations is an intriguing question which still remains to be completely understood. The transition between ordered and disordered phases in magnets, superfluids, charge density waves, etc., are typically studied within lattice models which assume the lattice to be static, both in the classical and quantum cases [1]. However, acoustic phonons are ubiquitous in realistic solid state systems, and their gaplessness gives reason to expect fundamental changes of the standard critical behavior.

The effect of phonons in classical phase transitions has been studied extensively and it was a topic of controversy for many years [2–11]. Using a simplified continuum model for the elastic lattice, Larkin and Pikin derived a criterion by which the second-order transition becomes first-order whenever the magnetic specific heat becomes large [5]. Intuitively, this results from the tendency of the system to gain energy by making distortions in the lattice. The Larkin-Pikin criterion has been used extensively in the literature in the study of different models [6–8]. This picture was revisited by Aharony [10], who showed through a renormalization group (RG) analysis in $d = 4 - \epsilon$ space dimensions that, contrary to the Larkin-Pikin criterion, the transition may remain second-order provided the phonon coupling is weak enough.

More recently, the focus has shifted to understanding the role of phonons in quantum phase transitions [12–16]. This is motivated by experiments on new platforms, such as interacting atoms, ions, and dipoles in a trap, which open possibilities to study quantum phase transitions in systems with soft lattices. On the solid state front, experiments on ferroelectric materials [17–21] further motivate this study. We note that

a prominent effect of the coupling to phonons is the explicit breaking of Lorentz invariance, which is often present in the effective field theory of the quantum $O(N)$ model. Lorentz violating terms of certain types have been shown to alter the critical behavior [22].

A number of theoretical analyses have looked at the quantum $O(N)$ model coupled to phonons in $D = 1 + 1$ space-time dimensions. An RG analysis was performed on a quantum wire [12], where it was shown that the transition could be second-order or first-order depending on the ratio of the spin-wave and phonon velocities. This analysis was extended in Ref. [14] and supplemented by a numerical verification using density matrix (RG) calculations [14]. Under specific conditions, the $1+1$ dimensional problem has been shown to

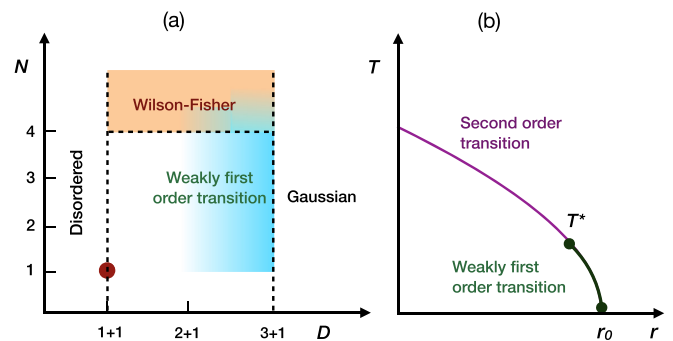


FIG. 1. (a) The nature of the quantum phase transition of the $O(N)$ model in presence of acoustic phonons is shown in the $N - D$ plane, where N is the number of flavors of the $O(N)$ spins and D is the space-time dimensions. We find a second-order transition (governed by Wilson-Fisher fixed point) for $N > 4$. The transition turns weakly first-order for $N \leq 4$. The quantum phase transition in $D = 1 + 1$ has been studied previously [12,14] (shown by a red point in the phase diagram). (b) We characterize the weakly first-order transition for $1 < N \leq 4$ by a length scale ξ^* , which can be related to a temperature scale T^* , below which the transition becomes first-order.

*abhiseks@campus.technion.ac.il

†Efrat.Shimshoni@biu.ac.il

‡podolsky@physics.technion.ac.il

support emergent supersymmetric quantum criticality [13,16]. However, understanding the effect of phonons on quantum criticality in higher dimensions remains a challenge.

Recently, the Larkin-Pikin criterion for magnetic transitions was generalized by including the quantum fluctuations [15]. There, it was shown that the universality of the Wilson-Fisher fixed point remains robust in $D = 3 + 1$, where the spin-phonon coupling term is argued to be marginally irrelevant. Below three space dimensions, however, such benign behavior of the coupling to phonons is no longer guaranteed.

In the present work, we show that phonons can indeed have a strong effects on quantum criticality below $D = 3 + 1$ dimensions. To this end we study the quantum $O(N)$ model weakly coupled to acoustic phonons by performing an RG analysis near $(3+1)$ dimensions, utilizing an ϵ expansion. Integrating out the phonons in our model leads to a nonlocal interaction in the effective action for the $O(N)$ order parameter field, which we analyze in detail. Our main finding is the presence of a critical number of flavors, $N_c = 4$: when the number of flavors N exceeds this value, the transition remains second-order governed by the standard Wilson-Fisher fixed point, while it turns weakly first-order below this critical number [Fig. 1(a)]. We characterize this weakly first-order transition by a length scale ξ^* , which diverges exponentially as ϵ approaches zero or the coupling to phonons becomes progressively smaller. This length scale can be heuristically related to the temperature scale T^* of a tricritical point, below which the transition turns from second-order to weakly first-order [Fig. 1(b)]. For the Ising model, $N = 1$, the divergent specific heat of the rigid-lattice model has been shown to lead to a thermal transition that is at least weakly first order [6]. Hence, the tricritical point in Fig. 1(b) is predicted to occur for $1 < N \leq 4$.

The rest of the paper is organized as follows: In Sec. II we introduce the coupled spin-phonon model, and derive an effective action for the spins resulting from integration over the phonons. In Sec. III we present the RG analysis of the effective action in $D = 3 + 1 - \epsilon$ dimensions, and derive the RG equations. In Sec. IV we show the solutions of the RG equations and discuss the results. Finally, in Sec. V we include a brief overview of our key results and concluding remarks.

II. COUPLED SPIN-PHONON MODEL

We consider a soft $O(N)$ quantum spin model in d space dimensions, with Euclidean action

$$\mathcal{S} = \int d\tau \left[\sum_i \left\{ (\partial_\tau \vec{\phi}_i)^2 + r \vec{\phi}_i^2 + \frac{U_0}{N} (\vec{\phi}_i^2)^2 \right\} - \sum_{\langle ij \rangle} J(\mathbf{R}_{ij}) \vec{\phi}_i \cdot \vec{\phi}_j \right], \quad (1)$$

where i and j are sites of the lattice, and we use arrows to indicate vectors in the internal $O(N)$ space and boldface letters to indicate vectors in real space. Here, J is the magnetic exchange between spins, which we assume to be dependent on the separation $\mathbf{R}_{ij} = \mathbf{R}_i - \mathbf{R}_j$ between nearest neighbors $\langle ij \rangle$. We also assume relativistic invariance (no first-order time derivatives) in the spin sector, as would be present, e.g., in Heisenberg ferromagnets or in non-particle-hole symmetric superfluids. For instance, Eq. (1) can describe Heisenberg antiferromagnets on bipartite lattices, with the field $\vec{\phi}$ representing the Néel vector.

We now introduce phonons by allowing the lattice to be dynamical. Then, the position at site i can be written in terms of the displacement \mathbf{u}_i from the equilibrium position $\mathbf{R}_i^{(0)}$ as $\mathbf{R}_i = \mathbf{R}_i^{(0)} + \mathbf{u}_i$. This gives rise to a quantum $O(N)$ model coupled to gapless phonons, in the form of the Wagner-Swift Hamiltonian [9,10]. The corresponding Euclidean action is given by

$$\mathcal{S} = \mathcal{S}_s + \mathcal{S}_p + \mathcal{S}_{sp}, \quad (2)$$

$$\mathcal{S}_s = \int d\tau \left[\sum_i \left\{ (\partial_\tau \vec{\phi}_i)^2 + r \vec{\phi}_i^2 + \frac{U_0}{N} (\vec{\phi}_i^2)^2 \right\} - J_0 \sum_{\langle ij \rangle} \vec{\phi}_i \cdot \vec{\phi}_j \right], \quad (3)$$

$$\mathcal{S}_p = \int d\tau \left[\frac{M}{2} \sum_i (\partial_\tau \mathbf{u}_i)^2 + \frac{1}{2} \sum_{\langle ij \rangle} \kappa_{ij}^{ab} u_i^a u_j^b \right], \quad (4)$$

$$\mathcal{S}_{sp} = \int d\tau \left[\sum_i \Psi_i^a u_i^a \right], \quad (5)$$

where $J_0 = J(\mathbf{R}_{ij}^{(0)})$ is independent of the bond $\langle ij \rangle$. In what follows, we adopt units where $J_0 = 1$. \mathcal{S}_p is the action of the harmonic phonons [Eq. (4)], where M is the mass of the atoms and $\kappa_{ij}^{ab} = \kappa^{ab}(\mathbf{R}_{ij}^{(0)})$ is the elastic tensor of the lattice. Here, we have expanded the spin-lattice interaction to first-order in the displacements \mathbf{u}_i . Therefore,

$$\Psi_i^a = - \sum_{\langle jl \rangle} \frac{\partial J(\mathbf{R}_{jl})}{\partial R_j^a} \Big|_{\mathbf{R}_j^{(0)}} \vec{\phi}_j \cdot \vec{\phi}_l. \quad (6)$$

A sum over repeated indices is implicit throughout the paper.

It is useful to write the action in Fourier space. To do so, we assume $J(\mathbf{R}_{ij}) = J(|\mathbf{R}_{ij}|)$ and define

$$g = \frac{\partial J(\mathbf{R}_{ij})}{\partial |\mathbf{R}_{ij}|} \Big|_{\mathbf{R}_{ij}^{(0)}}, \quad (7)$$

which is independent of the bond $\langle ij \rangle$ and plays the role of the spin-phonon coupling constant. Then, the Fourier transform of $\Psi_i^a(\tau)$ becomes

$$\Psi^a(\mathbf{q}, \omega) = -g \sum_{\langle ij \rangle} e^{i\mathbf{q} \cdot \mathbf{R}_i^{(0)}} (1 - e^{-i\mathbf{q} \cdot \mathbf{R}_j^{(0)}}) \frac{R_{ij}^a(0)}{|\mathbf{R}_{ij}^{(0)}|} \vec{\phi}_i \cdot \vec{\phi}_j = \frac{g}{2} \int \frac{d\omega'}{2\pi} \sum_{\mathbf{k}, \mu} \mu^a (e^{-i(\mathbf{q}-\mathbf{k}) \cdot \mu} - e^{i\mathbf{k} \cdot \mu}) \vec{\phi}(\mathbf{k}, \omega') \cdot \vec{\phi}(\mathbf{q} - \mathbf{k}, \omega - \omega'), \quad (8)$$

where $\vec{\phi}(\mathbf{k}, \omega)$ are the Fourier components of $\vec{\phi}_i(\tau)$, and μ is a shift by one lattice site in different directions. Let us take an example of the square lattice, for which $\mu \in \{\pm\hat{x}, \pm\hat{y}\}$ in units where the lattice spacing is one. Then

$$\Psi^a(\mathbf{q}, \omega) = -g \int \frac{d\omega'}{2\pi} \sum_{\mathbf{k}} i(\sin(q_a - k_a) + \sin k_a) \vec{\phi}(\mathbf{k}, \omega') \cdot \vec{\phi}(\mathbf{q} - \mathbf{k}, \omega - \omega'), \quad (9)$$

which in the small k and q limit reduces to the following form:

$$\Psi^a(\mathbf{q}, \omega) = -igq_a \int \frac{d\omega'}{2\pi} \sum_{\mathbf{k}} \vec{\phi}(\mathbf{k}, \omega') \cdot \vec{\phi}(\mathbf{q} - \mathbf{k}, \omega - \omega'). \quad (10)$$

Note that the $O(N)$ fields couple to the phonons only via the spatial derivatives, which appear in Eq. (10) as a spatial momentum factor q_a . This will lead to Lorentz symmetry breaking in the resulting effective quantum spin model.

Since we are considering a quadratic theory for the phonons, we can integrate them out to get an effective action for the spins. This will come at the cost of making the effective spin interaction nonlocal. The effective action for the spins is $\mathcal{S}_s^{\text{eff}} = \mathcal{S}_s + \delta\mathcal{S}_s$, where

$$\mathcal{S}_s = \int \frac{d\omega}{2\pi} \sum_{\mathbf{k}} (r + \omega^2 + v^2\mathbf{k}^2) \vec{\phi}(\mathbf{k}, \omega) \cdot \vec{\phi}(-\mathbf{k}, -\omega) + \frac{U_0}{N} \int \frac{d\omega}{2\pi} \sum_{\mathbf{q}} \left| \int \frac{d\omega'}{2\pi} \sum_{\mathbf{k}} \vec{\phi}(\mathbf{k}, \omega') \cdot \vec{\phi}(\mathbf{q} - \mathbf{k}, \omega - \omega') \right|^2, \quad (11)$$

and

$$\delta\mathcal{S}_s = \int \frac{d\omega}{2\pi} \sum_{\mathbf{q}} \sum_{ab} \frac{\Psi^a(\mathbf{q}, \omega) \Psi^b(-\mathbf{q}, -\omega)}{[M\omega^2\delta^{ab} + \kappa^{ab}(\mathbf{q})]} \approx - \int \frac{d\omega}{2\pi} \sum_{\mathbf{q}} \frac{g^2\mathbf{q}^2}{M(\omega^2 + c^2\mathbf{q}^2)} \left| \int \frac{d\omega'}{2\pi} \sum_{\mathbf{k}} \vec{\phi}(\mathbf{k}, \omega') \cdot \vec{\phi}(\mathbf{q} - \mathbf{k}, \omega - \omega') \right|^2, \quad (12)$$

where the last step was obtained assuming the elastic tensor $\kappa^{ab}(\mathbf{q}) = Mc^2q^aq^b + Mv_T^2(q^2\delta^{ab} - q^aq^b)$, with c and v_T the longitudinal and transverse phonon velocities, respectively. Note that the transverse phonons drop out of the above expression and we end up with $\delta\mathcal{S}_s$ written only in terms of the longitudinal phonon velocity c , which we assume to be isotropic in all spatial directions. The partition function is therefore given by (up to an overall constant),

$$Z = \int \mathcal{D}\phi e^{-S[\phi]} = \int \mathcal{D}\phi \exp \left[-\frac{1}{2} \int_{\omega, \mathbf{k}} (r + \omega^2 + v^2\mathbf{k}^2) \vec{\phi}(\mathbf{k}, \omega) \cdot \vec{\phi}(-\mathbf{k}, -\omega) - \frac{1}{N} \int_{\omega, \mathbf{q}} \int_{\omega_1, \mathbf{k}_1} \int_{\omega_2, \mathbf{k}_2} \left(U_0 + W \frac{c^2\mathbf{q}^2}{\omega^2 + c^2\mathbf{q}^2} \right) \phi^\alpha(\mathbf{k}_1, \omega_1) \phi^\alpha(-\mathbf{k}_1 - \mathbf{q}, -\omega_1 - \omega) \phi^\beta(\mathbf{k}_2 + \mathbf{q}, \omega_2 + \omega) \phi^\beta(-\mathbf{k}_2, -\omega_2) \right], \quad (13)$$

where $W = -\frac{g^2N}{M} < 0$, and we have used the shorthand notations $\int_{\omega, \mathbf{k}} = \int_{-\infty}^{\infty} \frac{d\omega}{2\pi} \int_{|\mathbf{k}| < \Lambda} \frac{d^d\mathbf{k}}{(2\pi)^d}$ and

$$\mathcal{D}\phi = \prod_{\omega} \prod_{|\mathbf{k}| < \Lambda} \prod_{\alpha=1}^N d\phi^\alpha(\mathbf{k}, \omega). \quad (14)$$

All momentum integrals are bounded by a cut-off Λ , set by the lattice spacing a , i.e., $\Lambda \sim \frac{1}{a}$. Notably, the resulting action does not have Lorentz invariance, as is reflected in the non-trivial (ω, \mathbf{q}) dependence of the interaction term W [Eq. (13)]. Therefore, the cutoff only applies to the wave vector, and we integrate over modes of all frequencies.

The W term provides a correction to the standard ϕ^4 -model which is nonlocal in space time. In momentum space, this is manifested by the dependence on transferred wave vector and frequency of the effective interaction

$$U_{\text{eff}}(\mathbf{q}, \omega) = U_0 + W \frac{c^2\mathbf{q}^2}{\omega^2 + c^2\mathbf{q}^2}. \quad (15)$$

Its naive scaling dimension at the Gaussian fixed point is the same as that of U_0 , i.e., $D - 4$ ($D = d + 1$ being the space-time dimension). Hence, the upper critical space-time dimension is 4, which implies that we can perform a controlled expansion in $\epsilon = 4 - D$ (or, equivalently,

$\epsilon = 3 - d$). However, the nonanalytical nature of $U_{\text{eff}}(\mathbf{q}, \omega)$ at $(\omega, \mathbf{q}) = 0$ (which exhibits a dependence on angle in the $\{|\mathbf{q}|, \omega\}$ -plane) forces a profound modification of the standard analysis [23–25], as detailed in the next section.

III. RENORMALIZATION GROUP PROCEDURE

A. Spherical harmonics decomposition

In Euclidean space time, the interaction in Eq. (15) decays as a power-law and depends on the angle relative to the time-like direction. This angular dependence exhibits a quadrupolar structure, parametrized by

$$\sin^2\theta = \frac{v^2\mathbf{q}^2}{\omega^2 + v^2\mathbf{q}^2}, \quad (16)$$

where v is the spin-wave velocity. To set the stage for a systematic RG analysis, we therefore perform a multipole expansion of U_{eff} in terms of spherical harmonics in D dimensions:

$$U_{\text{eff}}(\mathbf{q}, \omega) = \sum_{n=0}^{\infty} u_n Y_n(\theta). \quad (17)$$

Recalling that we focus on $D = 4 - \epsilon$ where the interaction parameters u_n near criticality are already of linear order in

ϵ , we use here the four-dimensional spherical harmonics Y_n (see Appendix A for details). Note that although the spin-wave velocity v flows under RG, the Gaussian part of the action [the quadratic part of Eq. (13)] is Lorentz invariant with respect to this velocity at every stage of the RG; hence it is natural to use the spherical harmonics expansion in terms of $\sin \theta$ as defined in Eq. (16). This approach is similar in spirit to the use of spherical harmonics in Ref. [11]. However, in our analysis the anisotropy is in the space vs time directions, arising from the Lorentz symmetry breaking.

When we perform the RG, we will find that higher even-order multipoles are generated at every step, which have the same naive scaling dimension. The coefficients u_n in Eq. (17) will therefore be considered as an infinite set of running parameters. Their bare values are given by

$$u_0 = \sqrt{2\pi} \left(U_0 + \frac{c(c+2v)}{(c+v)^2} W \right) \quad (18)$$

for $n = 0$ and

$$u_n = -\frac{2\sqrt{2}c\pi cv^2(c-v)^{n-1}}{(c+v)^{n+2}} W \quad (19)$$

for $n \geq 1$. They exhibit a systematic suppression by a velocity mismatch factor for increasing n :

$$\frac{u_{n+1}}{u_n} = \frac{c-v}{c+v}. \quad (20)$$

Note that for $c > v$, $W < 0$ and $U_0 > 0$ imply that $u_n > 0$ for all n . For $c < v$, u_n of even and odd n have alternating signs for $n \geq 1$; however, the leading phonon-induced coupling u_1 is always positive, as is u_0 .

B. Derivation of RG equations

We now perform an RG scaling transformation following the ϵ expansion approach [23–25]. To this end we define a momentum shell

$$\frac{\Lambda}{b} < |\mathbf{k}| < \Lambda, \quad (21)$$

which corresponds to the high wave vector (short wavelength) fluctuations. We will denote momenta in this shell by $\mathbf{k}^>$, and momenta $|\mathbf{k}| < \Lambda/b$ by $\mathbf{k}^<$. We then divide the integrals over the fields $\phi^\alpha(\mathbf{k}, \omega)$ into fast and slow modes, $\phi^>$ and $\phi^<$, corresponding to modes with momenta $\mathbf{k} \in \mathbf{k}^>$ and $\mathbf{k} \in \mathbf{k}^<$, respectively. Integration over the fast modes yields an effective action $S_{\text{eff}}[\phi^<]$ for the slow modes, given by

$$e^{-S_{\text{eff}}[\phi^<]} = \int \mathcal{D}\phi^> e^{-S[\phi^>, \phi^<]}, \quad (22)$$

where $\mathcal{D}\phi^> = \prod_\omega \prod_{\mathbf{k} \in \mathbf{k}^>} \prod_{\alpha=1}^N d\phi^\alpha(\mathbf{k}, \omega)$. The interaction U_{eff} in Eq. (15) gives rise to the Feynman rules shown in Fig. 2(a). Let us first consider the renormalization of the terms in the action that are quadratic in $\phi^<$. These come from the Feynman diagrams shown in Figs. 2(b) and 2(c), which we denote by I_1 and I_2 . They are given by

$$I_1 = 2 \int_{\omega, \mathbf{k}^>} \frac{U_{\text{eff}}(\mathbf{0}, 0)}{r + \omega^2 + v^2 \mathbf{k}^2}, \quad (23)$$

$$I_2(\mathbf{k}, \omega) = 4 \frac{1}{N} \int_{\omega', \mathbf{k}'^>} \frac{U_{\text{eff}}(\mathbf{k} + \mathbf{k}', \omega + \omega')}{r + \omega'^2 + v^2 \mathbf{k}'^2}. \quad (24)$$

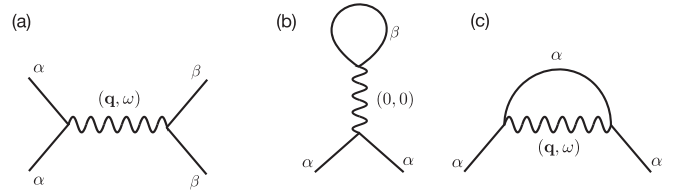


FIG. 2. (a) Feynman diagram corresponding to the interaction term in the action [Eq. (13)]. Here the wiggly lines represent the effective interaction $\frac{1}{N} U_{\text{eff}}(\mathbf{q}, \omega)$ [Eq. (15) in the text]. The indices α, β correspond to different flavors of the $O(N)$ -field propagators. (b), (c) Feynman diagrams responsible for the renormalization of the terms quadratic in ϕ in the action [Eq. (13)]. There are two possible diagrams, denoted I_1 (b) and I_2 (c). Note that I_2 depends on the transferred momentum and frequency (\mathbf{q}, ω) .

Note that I_1 [Eq. (23)] involves the interaction exactly at $(\mathbf{q} = 0, \omega = 0)$. In our case, this is ill-defined, since $U_{\text{eff}}(\mathbf{k}, \omega)$ depends on the direction in which the origin is approached. Hence, we replace it by the spherical average over all directions, $\int 4\pi \sin^2(\theta) d\theta U_{\text{eff}}(\theta) = 2\pi^2 u_0$.

To leading order in the ϵ expansion, we can set $d = 3$ while evaluating I_1 and I_2 and we find

$$I_1 = \frac{u_0}{4\pi^2 v^3} (2v^2 \Lambda^2 - r) \left(1 - \frac{1}{b} \right), \quad (25)$$

$$I_2(\mathbf{k}, \omega) = \frac{1}{2\pi^2 v^3 N} \left[(2v^2 \Lambda^2 - r) u_0 + 2v^2 \Lambda^2 \sum_{n=1}^{\infty} u_n + \frac{1}{3} (3\omega^2 - v^2 k^2) u_1 \right] \left(1 - \frac{1}{b} \right),$$

$$\equiv I_2(0, 0) + A(3\omega^2 - v^2 k^2)$$

$$\text{where } A \equiv \frac{1}{N} \frac{u_1}{6\pi^2 v^3} \left(1 - \frac{1}{b} \right). \quad (26)$$

Note that I_2 is momentum and frequency dependent. The expression in Eq. (26) was obtained by evaluating the integral in Eq. (24) and then Taylor expanding it to order k^2 and ω^2 . Higher-order terms were discarded, since they are irrelevant in the RG sense. Note that, despite the nonlocal nature of the phonon-mediated interaction, the shell integration of short-scale fluctuations leaves the kernel I_2 local, i.e., analytic in small k and ω , thus justifying the use of a Taylor series. In the leading order in ϵ , the frequency and momentum dependence

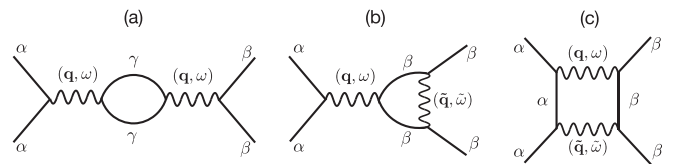


FIG. 3. Feynman diagrams arising from the renormalization of the quartic interaction terms in the action [Eq. (13)]. Panels (a), (b), and (c) depict the three possible diagrams, denoted D_1 , D_2 , and D_3 respectively. While evaluating them, we set all external momenta to zero.

in Eq. (26) is only associated with the interaction u_1 . This term leads to renormalization of the spin-wave velocity v .

Next, we will consider the renormalization of the quartic interaction. This comes from three diagrams, shown in Fig. 3, which we denote by D_1 , D_2 , and D_3 . Once again

accounting for the leading order in ϵ , we calculate $D_{\{1,2,3\}}$ in three dimensions ($d = 3$). Additionally, we set all external momenta to zero since any momentum dependence in D_i 's will be irrelevant, by power counting. Using these, we find (see Appendix B for details)

$$D_1 = \frac{1}{\pi^2 v^3 N} \sum_{l,m=0}^{\infty} u_l u_m \sum_{n=|l-m|}^{l+m} Y_n(\theta) \left(1 - \frac{1}{b}\right), \quad (27)$$

$$D_2 = \frac{4}{\pi^2 v^3 N^2} u_0 \sum_{n=0}^{\infty} u_n Y_n(\theta) \left(1 - \frac{1}{b}\right), \quad (28)$$

$$D_3 = \frac{4}{\pi^2 v^3 N^2} \sum_{n=0}^{\infty} u_n^2 \left(1 - \frac{1}{b}\right). \quad (29)$$

Note that while evaluating the diagrams, we have used the fact that the product of two spherical harmonics is also a linear combination of spherical harmonics with the coefficients listed in Appendix A. Also note that while the result for D_3 contains only the zeroth harmonics Y_0 [Eq. (29)], the diagrams D_1 and D_2 generate an infinite number of spherical harmonics [Eqs. (27) and (28)]. However, since the higher harmonics are more rapidly oscillating, we work with up to the second harmonics Y_2 , truncating for now the higher harmonics. Notably, we will show below that to leading order in the ϵ expansion, corrections arising from these higher harmonics do not alter the critical behavior.

Now incorporating the contributions from the one-loop diagrams, we can write the partition function as

$$\begin{aligned} Z = \mathcal{N} \int \mathcal{D}\phi^{\leq} \exp \left[-\frac{1}{2} \int_{\omega, \mathbf{k}^{\leq}} \{r + \omega^2 + v^2 \mathbf{k}^2 + 2(I_1 + I_2(0, 0) + A(3\omega^2 - v^2 k^2))\} \phi^{\leq \alpha}(\mathbf{k}, \omega) \phi^{\leq \alpha}(-\mathbf{k}, -\omega) \right. \\ \left. - \frac{1}{N} \int_{\omega, \mathbf{q}^{\leq}} \int_{\omega_1, \mathbf{k}_1^{\leq}} \int_{\omega_2, \mathbf{k}_2^{\leq}} \left(U_{\text{eff}}(\mathbf{q}, \omega) - \frac{N}{2} (D_1 + D_2 + D_3) \right) \phi^{\leq \alpha}(\mathbf{k}_1, \omega_1) \phi^{\leq \alpha}(-\mathbf{k}_1 - \mathbf{q}, -\omega_1 - \omega) \phi^{\leq \beta} \right. \\ \left. \times (\mathbf{k}_2 + \mathbf{q}, \omega_2 + \omega) \phi^{\leq \beta}(-\mathbf{k}_2, -\omega_2) \right]. \quad (30) \end{aligned}$$

We then rescale (\mathbf{k}, ω) according to

$$\mathbf{k} = b^{-1} \mathbf{k}' \quad \omega = b^{-1} \omega' \quad (31)$$

which ensures that the upper bound of \mathbf{k} is restored back to Λ . We subsequently rescale the fields ϕ^{\leq} according to

$$\phi = b^{(d+3)/2} (1 + 6A)^{-\frac{1}{2}} \phi' \quad (32)$$

in order to keep the coefficient of ω^2 in Eq. (30) the same as in the original theory. Note that the factor A is proportional to u_1 [Eq. (26)], which governs the correction to the scaling dimension arising from the spin-phonon coupling. We will discuss this in detail in the Results section.

Using these rescalings in Eq. (30), and setting $b = (1 + dl)$, we obtain the RG equations to the leading order in ϵ as given in Appendix C:

$$\frac{dr}{dl} = 2r + \frac{1}{2} \left(1 + \frac{2}{N}\right) (2v^2 \Lambda^2 - r) w_0 + \frac{2v^2 \Lambda^2 - r}{N} w_1 + \frac{2v^2 \Lambda^2}{N} w_2, \quad (33)$$

$$\frac{dv}{dl} = -\frac{1}{N} \frac{2v w_1}{3}, \quad (34)$$

$$\frac{dw_0}{dl} = \epsilon w_0 - \frac{1}{2} \left(1 + \frac{8}{N}\right) w_0^2 - \frac{1}{2} \left(1 + \frac{8}{3N}\right) w_1^2 - \frac{1}{2} \left(1 + \frac{4}{N}\right) w_2^2, \quad (35)$$

$$\frac{dw_1}{dl} = \epsilon w_1 - \left(1 + \frac{2}{N}\right) w_0 w_1 - \frac{1}{2} \left(1 - \frac{2}{3N}\right) w_1^2 - \frac{1}{2} w_2^2 - \left(1 - \frac{1}{N}\right) w_1 w_2, \quad (36)$$

$$\frac{dw_2}{dl} = \epsilon w_2 - \left(1 + \frac{2}{N}\right) w_0 w_2 - \frac{1}{2} \left(1 + \frac{2}{3N}\right) w_1^2 - \frac{1}{2} w_2^2 - \left(1 - \frac{1}{3N}\right) w_1 w_2. \quad (37)$$

Here, the new variables w_n are directly related to the interaction parameters u_n via a velocity-dependent rescaling:

$$w_n \equiv \frac{u_n}{\pi^2 v^3}, \quad (38)$$

which simplifies the form of the final equations.

Note that the equations for the w 's do not depend on the other two parameters, r and v , and hence close among themselves. Therefore, we can separately study the RG equations for the w 's, but keep in mind that at every RG stage, the solutions for the w 's impact the flow of r and v . In the above RG equations, we truncated by eliminating the dependence on w_3, w_4 and so on [Eqs. (33)–(37)]. However, one can show that for all $n \geq 1$,

$$\frac{dw_n}{dl} = \epsilon w_n - \left(1 + \frac{2}{N}\right) w_0 w_n + \dots, \quad (39)$$

where \dots stands for terms that are bilinear in w_l with $l \geq 1$. Later we will argue that the truncation will not affect our conclusions and we will discuss the relevance of Eq. (39).

Recalling that the bare value of w_1 is positive (since $W < 0$), Eq. (34) implies that the spin-wave velocity is initially renormalized downwards. In practice, we find that w_1 does not change sign, hence this trend is maintained throughout the flow, and is only stopped in cases where w_1 flows to zero.

IV. RESULTS

When $W = 0$, as is the case in the absence of phonons, all harmonics, except for w_0 , vanish and the RG equations reduce to those of the standard $O(N)$ model. The underlying relativistic invariance then prevents w_n with $n \geq 1$ from being generated in the RG flow. Therefore the Wilson-Fisher (WF) fixed point

$$v^* = v_{\text{in}} \text{ (initial value)}, \quad (40)$$

$$r^* = -\left(\frac{N+2}{N+8}\right) v_{\text{in}}^2 \Lambda^2 \epsilon, \quad (41)$$

$$w_0^* = \left(\frac{2N}{N+8}\right) \epsilon, \quad (42)$$

$$w_n^* = 0 \quad \text{for } n \geq 1, \quad (43)$$

remains a fixed point of Eqs. (33)–(37), although its stability can be affected by the phonon coupling. We note that the renormalized velocity, v^* , is not universal at the fixed point.

In order to determine whether the WF fixed point is stable to the addition of spin-phonon interactions, we linearize the RG equations around the fixed point, and obtain (considering up to w_2)

$$\frac{d}{dl} \begin{bmatrix} \delta r \\ \delta v \\ \delta w_0 \\ \delta w_1 \\ \delta w_2 \end{bmatrix} = \begin{bmatrix} 2 - \frac{N+2}{N+8} \epsilon & 4\left(\frac{N+2}{N+8}\right) v^* \Lambda^2 \epsilon & \left(1 + \frac{2}{N}\right) \left(1 + \frac{N+2}{2(N+8)} \epsilon\right) v^{*2} \Lambda^2 & \frac{2}{N} \left(1 + \frac{N+2}{2(N+8)} \epsilon\right) v^{*2} \Lambda^2 & \frac{2v^{*2} \Lambda^2}{N} \\ 0 & 0 & 0 & -\frac{2v^*}{3N} & 0 \\ 0 & 0 & -\epsilon & 0 & 0 \\ 0 & 0 & 0 & \frac{4-N}{N+8} \epsilon & 0 \\ 0 & 0 & 0 & 0 & \frac{4-N}{N+8} \epsilon \end{bmatrix} \begin{bmatrix} \delta r \\ \delta v \\ \delta w_0 \\ \delta w_1 \\ \delta w_2 \end{bmatrix}. \quad (44)$$

Since the matrix is upper-triangular, the eigenvalues are given by the diagonal elements. In fact, based on Eq. (39) one can see that the upper-triangular structure of the matrix is preserved when all w_n s are kept and no truncation is done. Then, the diagonal element corresponding to δw_n takes the value

$$\frac{4-N}{N+8} \epsilon \quad (45)$$

for all $n \geq 1$. This demonstrates that $N = 4$ is special, and that the WF fixed point is stable for $N > 4$ and unstable for $N < 4$. We will next consider the cases $N > 4$ and $N < 4$ separately.

A. Case $N > 4$

For $N > 4$, the WF fixed point is stable. Since δw_n decays exponentially with l for all $n \geq 1$, w_n is marginally irrelevant and the WF fixed point is robust against small spin-phonon coupling.

We furthermore argue that the critical exponents are identical to the standard $O(N)$ model. To see this, note that the matrix in Eq. (44) is upper triangular, and therefore its eigenvalues are given by its diagonals. In particular, the scaling dimension of $r, \gamma_r = 2 - \frac{N+2}{N+8} \epsilon$, yields the known value for the correlation length exponent ν . Then, the remaining exponents

(β, γ , etc.), can be deduced from the scaling of the field ϕ [Eq. (32)]. This differs from the WF by a factor dependent on A which in turn is proportional to w_1 [Eq. (26)]. Since $w_1^* = 0$, this reduces to the standard scaling of the $O(N)$ model.

B. Case $N < 4$

For $N < 4$, w_n is relevant and hence starting from a small initial positive value $w_{n\text{in}}$ it grows rapidly for all $n \geq 1$. Note that all w_n have a similar behavior, however in the following discussion we will mainly focus on w_1 since it corresponds to the leading spin-phonon coupling. In order to search for a fixed point that describes the new critical point, we solve the RG equations and find that one of the fixed points is the WF one as described in Eqs. (40)–(43). We find that, regardless of the initial values of the parameters, the RG equations become unstable, indicating a first-order transition. The source of this instability is that, even for arbitrarily small initial value $w_{1\text{in}}$, w_1 eventually grows rapidly and drives w_0 to become negative – see the last two terms in Eq. (35). Once w_0 is negative, the ϕ^4 theory collapses.

Nevertheless, for $w_{1\text{in}}$ sufficiently close to $w_1^* = 0$, the WF fixed point still plays an important role. Then, w_1 remains

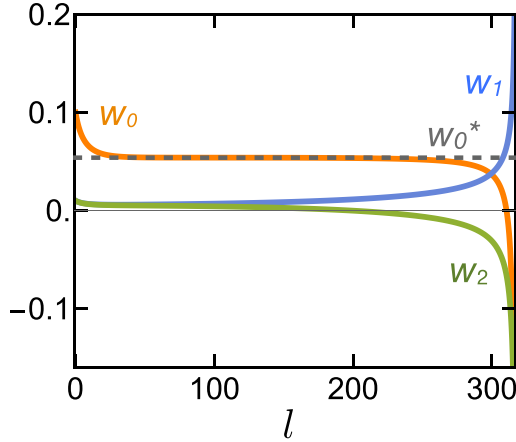


FIG. 4. The flow of w_0 , w_1 , and w_2 are shown as a function of RG time l , along with the Wilson-Fisher value of w_0 , i.e., w_0^* for $N = 3$. Starting from an initial value of $w_{0\text{in}} = 0.1$, it first decays exponentially and reaches a constant value. w_1 on the other hand starts from a small positive value ($w_{1\text{in}} = 0.01$), then grows fast and eventually pulls w_0 to a negative value. w_2 also starts from the same initial value $w_{2\text{in}} = 0.01$, but it turns to a negative value and diverges near the instability. w_0 spends a long time at its Wilson-Fisher value showing a plateau. We define a characteristic scale l^* where the above described breakdown occurs (see text).

small for a long RG time l , during which its effect on other parameters can be neglected. As a result, w_0 flows towards its WF value w_0^* , and stays there for a long time, as shown in Fig. 4. Eventually, when w_1 grows sufficiently, it pulls w_0 to negative values, at which point the RG equations become unstable.

The fact that the system spends a long time near the fixed point implies that the transition is weakly first-order. This follows since the value l^* of the RG parameter l at the instability is large, and therefore the characteristic scale $\xi^* \sim e^{l^*}$ at the instability is also large. The picture that then emerges is that, as one approaches the phase transition between ordered and disordered phases, the correlation length grows following the standard WF exponent. However, close enough to the transition, the divergence in the correlation length is cut off by the scale ξ^* . Thus, ξ^* provides the characteristic correlation length at the first-order transition.

Here we provide an estimate for the correlation length ξ^* . We note that the instability occurs when w_1 grows and becomes roughly equal to w_0^* . We assume that starting from a small initial value $w_{1\text{in}}$, w_1 grows exponentially (as in its linear order)

$$w_1 = w_{1\text{in}} e^{\frac{(4-N)}{(N+8)} \epsilon l}, \quad (46)$$

until the system reaches this instability. Using this, we obtain the estimated correlation length

$$\xi^* = a e^{l^*} \approx a \left[\frac{2N}{N+8} \frac{\epsilon}{w_{1\text{in}}} \right]^{\frac{(N+8)}{(4-N)} \frac{1}{\epsilon}}, \quad (47)$$

where a is the lattice constant. We have checked that for small ϵ and small $w_{1\text{in}}$, this analytic estimate of the correlation length is consistent with the length scale obtained from numerics, at which the value of v sharply falls to zero, and w_0 and w_1 diverge.

The weakly first-order transition in the presence of spin-phonon coupling can be characterized by this length-scale ξ^* . For system sizes up to this length scale the system exhibits correlations and scaling consistent with the Wilson-Fisher second-order transition. Beyond that scale, a weakly first-order transition is manifested. From Eq. (47), we see that ξ^* grows exponentially when either ϵ or the coupling to phonons become smaller. Note that the picture remains qualitatively same when including higher harmonics in the RG equations.

Although the quantum critical point is strictly defined at zero temperature, in any physical realization there is a finite temperature which is related to the finite size in the Euclidean time direction. Therefore, there is a temperature scale T^* associated with this length scale, given by $T^* \sim \frac{\hbar v}{k_B \xi^*}$. Above this temperature, the quantum RG flow is cut off by the finite size in the time direction while w_1 is still small and w_0 is still positive. Then, the system is described by a thermal transition in $d = 3 - \epsilon$ space dimensions, which for small enough w_1 may result in a second-order transition [10]. T^* is therefore the temperature of the tricritical point separating second-order and weakly first-order transitions [see Fig. 1(b)].

Finally, we consider the situation where the number of flavors is exactly 4 ($N = 4$). In this marginal case, we numerically find that the transition is always weakly first-order, no matter how weak $w_{1\text{in}}$ is. This is consistent with the observation that, even for $N > 4$, the transition becomes first-order whenever $w_{1\text{in}}$ exceeds some N -dependent threshold value $w_{1\text{thr}}(N)$. We find that, as N approaches four from above, $w_{1\text{thr}}(N)$ approaches zero, indicating that at $N = 4$ the second-order transition is first-order even for infinitesimal phonon coupling.

C. Other fixed points

We now consider the other possible fixed points, which are different from the Wilson-Fisher one. We find that additional fixed points do exist, but they are unstable and therefore do not play an important role in the RG, as explained below.

We first consider two RG equations Eqs. (35) and (36) in the absence of w_2 . We can analytically solve these two equations to obtain the fixed points:

$$w_0^{*(\pm)} = \frac{N(196 + 156N + 45N^2 \pm \sqrt{5(2 - 3N)\sqrt{9N^2 - 12N - 76}}\epsilon)}{416 + 436N + 300N^2 + 45N^3} \quad (48)$$

$$w_1^{*(\pm)} = 2 \frac{\epsilon - \left(1 + \frac{2}{N}\right) w_0^{*(\pm)}}{\left(1 - \frac{2}{3N}\right)}. \quad (49)$$

Note that these two fixed points are real when the number of flavors is larger than a critical number obtained by solving the equation $9\tilde{N}_c^2 - 12\tilde{N}_c - 76 = 0$, i.e., $N > \tilde{N}_c \approx 3.64$. We numerically find that the fixed point $\text{FP}^{(+)}$ is unstable in both directions for all $N > \tilde{N}_c$. On the other hand, the fixed point $\text{FP}^{(-)}$ starts from a positive value of w_1^* at $N = \tilde{N}_c$, coincides with the WF fixed point at $N = 4$ (with $w_1^* = 0$), and turns negative thereafter. We also notice that this fixed point is stable in both directions in the $\{w_0, w_1\}$ plane in the range $\tilde{N}_c < N < 4$.

These results relate to the truncated model with two interaction parameters (w_0 and w_1), but adding extra parameters could give rise to unstable directions. To test this, we add the higher-order harmonic w_2 , and numerically find the new fixed points [to Eqs. (35)–(37)] and study their stability. We still find two fixed points. However, with the addition of the third parameter w_2 , the value of \tilde{N}_c decreases to 2.48, and an unstable direction appears in the $\text{FP}^{(-)}$ fixed point. We find no reason to expect that the conclusion might change by adding higher-order harmonics, as this increases the potential for more unstable directions. We therefore conclude that there is no stable fixed point in the system apart from the WF fixed point for $N > 4$.

D. Cubic anisotropy

One can also consider various generalizations to our analysis. For instance, consider the effect of adding a cubic anisotropy term to the action [26–29],

$$S_{\text{cubic}} = \frac{\lambda}{N} \int d\tau \sum_i \sum_{\alpha} (\phi_i^{\alpha})^4. \quad (50)$$

This term breaks the $O(N)$ symmetry to a discrete N -dimensional hypercubic symmetry. One possible reason for the appearance of this cubic anisotropy term might be crystal field effects in magnets.

In Appendix D we repeat the RG analysis in this case. We find that adding a cubic-anisotropy term in the action changes the nature of the second-order transition for $N > 4$ from Wilson-Fisher to the standard (phononless) cubic universality class [26]. By contrast, for $N \leq 4$, the transition remains weakly first order, due to the coupling to phonons.

V. SUMMARY AND OUTLOOK

In summary, using renormalization group analysis in $4 - \epsilon$ dimensions, we have studied the quantum phase transition in the presence of acoustic phonons. We have shown that when the number of flavors of the underlying $O(N)$ model is larger than a critical number $N_c = 4$, the transition remains a standard second-order one. On the other hand when $N < N_c$, the transition becomes weakly first order, characterized by a large length scale ξ^* or, equivalently, by a small temperature scale below which the transition changes from second-order to first-order. We are currently in the process of verifying these analytical predictions numerically, using Monte Carlo simulations of $O(N)$ models coupled to phonons.

In principle, anharmonic corrections to the phonons arising from their coupling to the $O(N)$ fields could lead to structural instabilities of the lattice. Throughout our analysis, we did

not consider this possibility. This is justified provided that the phonons are stiff enough and the coupling to phonons is not too strong. However, it would be interesting to understand situations where these assumptions may break down, e.g., for systems near structural transitions [30,31] where the phonons are softened and susceptible to nonlinear corrections arising from coupling to the $O(N)$ fluctuations. Indeed, when the coupling to the phonons is strong enough, new phases involving structural reorganization of the lattice can occur. For example, in Ref. [32] this was demonstrated for an Ising model strongly coupled to optical phonons. It would be interesting to understand how this feedback can affect critical properties. Finally, even more dramatic effects of the coupling to the lattice can occur near melting transitions, where topological defects of the lattice can have an important interplay with the magnetic degrees of freedom [33,34].

ACKNOWLEDGMENTS

The authors acknowledge helpful discussions with A. Aharony, E. Altman, P. Chandra, S. Gazit, and A. Paramekanti. D.P. thanks the Israel Science Foundation for financial support (Grant No. 1803/18). E.S. thanks the Aspen Center for Physics (NSF Grant No. 1066293) for its hospitality, and financial support by the US-Israel Binational Science Foundation through awards No. 2016130 and 2018726, and by the Israel Science Foundation (ISF) Grant No. 993/19.

APPENDIX A: SPHERICAL HARMONICS IN (3+1) DIMENSIONS

We introduce the even-order spherical harmonics in four dimensions ($D = d + 1 = 4$), the first few of which are

$$\begin{aligned} Y_0(\theta) &= 1, \\ Y_1(\theta) &= -4 \sin^2 \theta + 3, \\ Y_2(\theta) &= 16 \sin^4 \theta - 20 \sin^2 \theta + 5, \\ Y_3(\theta) &= -64 \sin^6 \theta + 112 \sin^4 \theta - 56 \sin^2 \theta + 7, \\ &\vdots \end{aligned} \quad (A1)$$

where θ is the angle relative to the vertical ω axis in the $(v|q|, \omega)$ plane,

$$\sin^2 \theta = \frac{v^2 \mathbf{q}^2}{\omega^2 + v^2 \mathbf{q}^2}. \quad (A2)$$

These functions are found constructively: we choose $Y_0(\theta) = 1$. Then, for $n > 1$, Y_n is an even polynomial in $\sin \theta$ of order $2n$, whose coefficients are fixed by orthonormalizing it with all Y_l of lower order,

$$(Y_l, Y_n) = \delta_{ln}. \quad (A3)$$

Here, the inner product of two real functions $f(\theta)$ and $g(\theta)$ is defined by

$$(f, g) \equiv \frac{2}{\pi} \int_0^{\pi} \sin^2 \theta d\theta f(\theta) g(\theta). \quad (A4)$$

Note that our integration measure

$$d\Omega = \frac{2}{\pi} \sin^2 \theta d\theta \quad (\text{A5})$$

differs from the standard integration measure for angular integrals in four dimensions, $4\pi \sin^2 \theta$, by an overall factor of $2\pi^2$. This choice is convenient as it simplifies many of the expressions that follow.

The functions Y_n depend only on θ , the angle from the timelike axis. In particular, they are $\text{SO}(3)_{\text{space}}$ invariant, i.e., they do not depend on the orientation in the three-dimensional (3D), spacelike, directions. Thus, these functions are the four-dimensional analogs of the azimuthally symmetric ($m=0$), even order, spherical harmonics in 3D, $Y_{\ell m}$, with $\ell=2n$ and $m=0$. There are also odd harmonics, involving odd powers of $\sin \theta$, and harmonics that are not $\text{SO}(3)_{\text{space}}$ -invariant. However, since the bare action is even under parity, and since it is SO_{space} invariant, these harmonics are not generated in the RG.

Using trigonometric identities, the functions above can be rewritten in a simple form:

$$\begin{aligned} Y_0(\theta) &= 1, \\ Y_1(\theta) &= 1 + 2 \cos(2\theta), \\ Y_2(\theta) &= 1 + 2 \cos(2\theta) + 2 \cos(4\theta), \\ &\vdots \\ Y_n(\theta) &= 1 + 2 \cos(2\theta) + \dots + 2 \cos(2n\theta). \end{aligned} \quad (\text{A6})$$

In this form, and writing the integration measure as $d\Omega = \frac{1}{\pi}(1 - \cos(2\theta))$, it is straightforward to show that the functions are an orthonormal set.

These functions can be used to expand any even, $\text{SO}(3)_{\text{space}}$ -invariant, function. Note that the product of two spherical harmonics $Y_l(\theta)Y_m(\theta)$ is itself another even, $\text{SO}(3)_{\text{space}}$ -symmetric function. Therefore, it can be expanded in terms of $Y_n(\theta)$ s,

$$Y_l(\theta)Y_m(\theta) = \sum_{n=0}^{\infty} a_{n;lm} Y_n(\theta). \quad (\text{A7})$$

One can show that the coefficients $a_{n;lm}$ are given by

$$a_{n;lm} = \begin{cases} 1 & \text{for } |l-m| \leq n \leq l+m \\ 0 & \text{otherwise.} \end{cases} \quad (\text{A8})$$

We now use these results to derive a number of relations which will be useful when computing Feynman diagrams. Expanding the interaction as a linear combination of the spherical harmonics,

$$U_{\text{eff}}(\mathbf{q}, \omega) = \sum_{n=0}^{\infty} u_n Y_n(\theta), \quad (\text{A9})$$

we obtain

$$\int d\Omega U_{\text{eff}}(\mathbf{q}, \omega) = u_0, \quad (\text{A10})$$

$$\int d\Omega (U_{\text{eff}}(\mathbf{q}, \omega))^2 = \sum_{n=0}^{\infty} u_n^2, \quad (\text{A11})$$

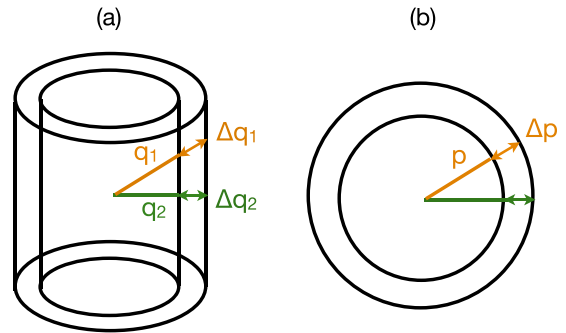


FIG. 5. (a) Cylindrical shell. We use an angle-dependent rescaling transformation, $p^\mu(\Omega) = g(\Omega)q^\mu$, and choose the rescaling function $g(\Omega)$ to deform the cylindrical shell to a spherical shell, shown in (b). Since $\frac{\Delta q_1}{q_1} = \frac{\Delta q_2}{q_2}$, the resulting spherical shell has constant thickness.

and

$$\begin{aligned} (U_{\text{eff}}(\mathbf{q}, \omega))^2 &= \sum_{l,m=0}^{\infty} u_l u_m Y_l(\theta) Y_m(\theta) \\ &= \sum_{l,m=0}^{\infty} u_l u_m \sum_{n=|l-m|}^{l+m} Y_n(\theta). \end{aligned} \quad (\text{A12})$$

We will use these results while evaluating the Feynman diagrams D_i 's.

APPENDIX B: EVALUATION OF THE FEYNMAN DIAGRAMS ARISING FROM THE RENORMALIZATION OF THE INTERACTION

Renormalization of the quartic interaction term in the action [Eq. (13)] comes from the diagrams D_1 , D_2 and D_3 shown in Fig. 3. Here we provide the integrals involved in those diagrams:

$$D_1(\mathbf{k}, \omega) = \frac{8}{N} (U_{\text{eff}}(\mathbf{k}, \omega))^2 \int_{\omega', \mathbf{k}'} \frac{1}{(r + \omega'^2 + v^2 \mathbf{k}'^2)^2}, \quad (\text{B1})$$

$$D_2(\mathbf{k}, \omega) = \frac{32}{N^2} U_{\text{eff}}(\mathbf{k}, \omega) \int_{\omega', \mathbf{k}'} \frac{U_{\text{eff}}(\mathbf{k}', \omega')}{(r + \omega'^2 + v^2 \mathbf{k}'^2)^2}, \quad (\text{B2})$$

$$D_3 = \frac{32}{N^2} \int_{\omega', \mathbf{k}'} \frac{U_{\text{eff}}(\mathbf{k}', \omega')^2}{(r + \omega'^2 + v^2 \mathbf{k}'^2)^2}. \quad (\text{B3})$$

In order to evaluate these integrals we set $r=0$, since it always contributes corrections $\sim \mathcal{O}(\frac{r}{\Lambda^2}) \ll 1$. We now introduce the Euclidean four-vector $q^\mu \equiv (\omega', v\mathbf{k}')$, and note that $U_{\text{eff}}(q^\mu)$ depends on the direction Ω of q^μ , but not on its magnitude, q . Then, one can see that all of the above integrals take the following form:

$$\int_{\text{cylinder}} \frac{d^4 q f(\Omega)}{q^4} = 2\pi^2 \int_{\text{cylinder}} d\Omega f(\Omega) \int \frac{dq q^3}{q^4} \quad (\text{B4})$$

integrated over the cylindrical shell in Fig. 5(a). In particular, the domain of the q integral depends on Ω .

We next introduce a direction-dependent scaling factor, $g(\Omega)$, and a rescaled variable $p^\mu = g(\Omega)q^\mu$, such that the cylindrical shell in q^μ , Fig. 5(a), is deformed to a spherical shell in p^μ , Fig. 5(b). Note that the thickness of the cylindrical shell, Δq , is proportional to the distance of the shell to the origin, q , such that if two different directions Ω_1 and Ω_2 are compared

$$\frac{\Delta q_1}{q_1} = \frac{\Delta q_2}{q_2}. \quad (\text{B5})$$

This implies that the spherical shell in Fig. 5(b) has constant thickness. Furthermore, since $\frac{dp}{p} = \frac{g(\Omega)dq}{g(\Omega)q} = \frac{dq}{q}$, the integral in Eq. (B4) becomes

$$\int_{\text{spher.shell}} d\Omega f(\Omega) \int \frac{dp}{p}. \quad (\text{B6})$$

In this form, the domain of integration is spherically symmetric. In particular, the domain of the p integral is independent of Ω , and can be evaluated directly

$$\int_{\Lambda/b}^{\Lambda} \frac{dp}{p} = \log b \approx 1 - \frac{1}{b} \quad (\text{B7})$$

where the final result is correct to linear order in $b - 1$ (which equals dl). Now, to compute the angular integral $\int d\Omega f(\Omega)$, all the results derived in Appendix A, Eqs. (A10)–(A12), can be used. Combining these results, we end up with the final answers for $D_{1,2,3}$ given in Eqs. (27)–(29) of the main text.

APPENDIX C: DERIVATION OF THE RG EQUATIONS

In this Appendix, we provide the intermediate steps to obtain the RG equations given in the main text [Eqs. (33)–(37)]. We apply the rescaling of (\mathbf{k}, ω) [Eq. (31)] and the scalar field [Eq. (32)] in Eq. (30). Then, comparing the coefficients of different parameters with those in Eq. (13), we obtain the following expressions for the renormalized parameters:

$$r' = \frac{b^2}{1 + 6A}(r + 2I_1 + 2I_2(0, 0)), \quad (\text{C1})$$

$$v'^2 = \left(\frac{1 - 2A}{1 + 6A} \right) v^2, \quad (\text{C2})$$

$$u'_0 = \frac{b^{3-d}}{(1 + 6A)^2} \left[u_0 - \frac{u_1}{v} \frac{dv}{dl} dl - \frac{1}{2\pi^2 v^3} \left\{ \left(1 + \frac{8}{N} \right) u_0^2 + \left(1 + \frac{4}{N} \right) (u_1^2 + u_2^2) \right\} \left(1 - \frac{1}{b} \right) \right], \quad (\text{C3})$$

$$u'_1 = \frac{b^{3-d}}{(1 + 6A)^2} \left[u_1 - \frac{u_1 + 3u_2}{2v} \frac{dv}{dl} dl - \frac{1}{2\pi^2 v^3} \left\{ \left(2 + \frac{4}{N} \right) u_0 u_1 + (u_1 + u_2)^2 \right\} \left(1 - \frac{1}{b} \right) \right], \quad (\text{C4})$$

$$u'_2 = \frac{b^{3-d}}{(1 + 6A)^2} \left[u_2 + \frac{u_1 - u_2}{2v} \frac{dv}{dl} dl - \frac{1}{2\pi^2 v^3} \left\{ \left(2 + \frac{4}{N} \right) u_0 u_2 + (u_1 + u_2)^2 \right\} \left(1 - \frac{1}{b} \right) \right]. \quad (\text{C5})$$

Note that the above renormalized parameters u'_n also include terms proportional to $\frac{dv}{dl}$. These arise due to the evolution of the harmonics Y_n as the spin-wave velocity changes with the RG flow, which is of the form

$$\left[\sum_{n=0}^{\infty} u_n Y_n \right]_{l+dl} = \left[\sum_{n=0}^{\infty} u_n Y_n \right]_l + \left[\sum_{n=0}^{\infty} u_n \frac{dY_n}{dv} \right]_l \frac{dv}{dl} dl, \quad (\text{C6})$$

and we use the identities $\frac{dY_0(\theta)}{dv} = 0$ and $\frac{dY_n(\theta)}{dv} = \frac{1}{2v} [-(n+1)Y_{n-1}(\theta) - Y_n(\theta) + nY_{n+1}(\theta)]$ (valid for $n \geq 1$) to evaluate the second term. Finally, setting $b = (1 + dl)$ and using the functional forms of A , I_1 and $I_2(0, 0)$ as given in Eqs. (25) and (26), lead to the following RG equations:

$$\frac{dr}{dl} = 2r + \left(1 + \frac{2}{N} \right) \frac{(2v^2 \Lambda^2 - r)u_0}{2\pi^2 v^3} + \frac{(2v^2 \Lambda^2 - r)u_1}{N\pi^2 v^3} + \frac{2\Lambda^2}{N\pi^2 v} u_2, \quad (\text{C7})$$

$$\frac{dv}{dl} = -\frac{1}{N} \frac{2u_1}{3\pi^2} \frac{1}{v^2}, \quad (\text{C8})$$

$$\frac{du_0}{dl} = \epsilon u_0 - \frac{1}{2\pi^2 v^3} \left(1 + \frac{8}{N} \right) u_0^2 - \frac{1}{N} \frac{2}{\pi^2 v^3} u_0 u_1 - \frac{1}{2\pi^2 v^3} \left(1 + \frac{8}{3N} \right) u_1^2 - \frac{1}{2\pi^2 v^3} \left(1 + \frac{4}{N} \right) u_2^2, \quad (\text{C9})$$

$$\frac{du_1}{dl} = \epsilon u_1 - \frac{1}{\pi^2 v^3} \left(1 + \frac{2}{N} \right) u_0 u_1 - \frac{1}{2\pi^2 v^3} \left(1 + \frac{10}{3N} \right) u_1^2 - \frac{1}{2\pi^2 v^3} u_2^2 - \frac{1}{\pi^2 v^3} \left(1 - \frac{1}{N} \right) u_1 u_2, \quad (\text{C10})$$

$$\frac{du_2}{dl} = \epsilon u_2 - \frac{1}{\pi^2 v^3} \left(1 + \frac{2}{N} \right) u_0 u_2 - \frac{1}{2\pi^2 v^3} \left(1 + \frac{2}{3N} \right) u_1^2 - \frac{1}{2\pi^2 v^3} u_2^2 - \frac{1}{\pi^2 v^3} \left(1 + \frac{5}{3N} \right) u_1 u_2. \quad (\text{C11})$$

Now we define $w_n = \frac{u_n}{\pi^2 v^3}$, which implies $\frac{dw_n}{dl} = \frac{1}{N} \frac{2u_1 u_n}{\pi^4 v^6} + \frac{1}{\pi^2 v^3} \frac{du_n}{dl}$, and using these the above equations simplify to Eqs. (33)–(37) in the main text.

APPENDIX D: INCLUSION OF CUBIC ANISOTROPY

In this Appendix we discuss the effect of a single-site term in the action [Eq. (3)] of the form $\frac{\lambda}{N} \int d\tau \sum_i \sum_{\alpha} (\phi_i^{\alpha})^4$, which breaks the $O(N)$ symmetry of the Hamiltonian [26] to a ‘‘cubic’’ symmetry. The presence of such a term in the action leads to additional contributions to the two-loop correction terms [Eqs. (27) and (28)] as follows:

$$D_1^{(\lambda)} = \frac{(1-1/b)}{\pi^2 v^3 N^2} \left[2\lambda \sum_{n=0}^{\infty} u_n Y_n(\theta) + \lambda^2 \delta_{\alpha\beta} \right], \quad (D1)$$

$$D_2^{(\lambda)} = \frac{4(1-1/b)}{\pi^2 v^3 N^2} \left[\lambda \sum_{n=0}^{\infty} u_n Y_n(\theta) + (\lambda u_0 + \lambda^2) \delta_{\alpha\beta} \right], \quad (D2)$$

$$D_3^{(\lambda)} = \frac{4(1-1/b)}{\pi^2 v^3 N^2} [2\lambda u_0 + \lambda^2] \delta_{\alpha\beta}. \quad (D3)$$

In these expressions, $\delta_{\alpha\beta}$ indicates contributions where all external lines in Fig. 3 have the same flavor. These terms renormalize λ .

Including these corrections, the RG equations [Eqs. (35)–(37)] are modified to the following set of equations, where we now have an additional equation for λ :

$$\begin{aligned} \frac{dw_0}{dl} &= \epsilon w_0 - \frac{1}{2} \left(1 + \frac{8}{N} \right) w_0^2 - \frac{1}{2} \left(1 + \frac{8}{3N} \right) w_1^2 \\ &\quad - \frac{1}{2} \left(1 + \frac{4}{N} \right) w_2^2 - \frac{3}{N} w_0 \lambda, \end{aligned} \quad (D4)$$

$$\begin{aligned} \frac{dw_1}{dl} &= \epsilon w_1 - \left(1 + \frac{2}{N} \right) w_0 w_1 - \frac{1}{2} \left(1 - \frac{2}{3N} \right) w_1^2 - \frac{1}{2} w_2^2 \\ &\quad - \left(1 - \frac{1}{N} \right) w_1 w_2 - \frac{3}{N} w_1 \lambda, \end{aligned} \quad (D5)$$

$$\begin{aligned} \frac{dw_2}{dl} &= \epsilon w_2 - \left(1 + \frac{2}{N} \right) w_0 w_2 - \frac{1}{2} \left(1 + \frac{2}{3N} \right) w_1^2 \\ &\quad - \frac{1}{2} w_2^2 - \left(1 - \frac{1}{3N} \right) w_1 w_2 - \frac{3}{N} w_2 \lambda, \end{aligned} \quad (D6)$$

$$\frac{d\lambda}{dl} = \epsilon \lambda - \frac{6}{N} w_0 \lambda + \frac{2}{N} w_1 \lambda - \frac{9}{2N} \lambda^2. \quad (D7)$$

Note that in the above equations, λ has been rescaled to include the $1/(\pi^2 v^3)$ factor. By setting the r.h.s of the above equations to zero we find several fixed points which we will discuss below:

(1) *Ising fixed point*: The Ising fixed point is given by $\lambda^* = \frac{2N}{9}\epsilon$ and $w_n^* = 0$ for all $n \geq 0$. This fixed point is unstable for all $N > 1$.

(2) *Wilson-Fisher fixed point*: The Wilson-Fisher fixed point as discussed in Eqs. (42) and (43) still remains a fixed point of the system with $\lambda^* = 0$. For $N > 4$ this fixed point is unstable to any finite λ , as in the phonon-less case [26].

(3) *Cubic fixed point*: There is a new cubic fixed point, given by $w_0^* = \frac{2\epsilon}{3}$, $\lambda^* = \frac{2(N-4)\epsilon}{3}$, and $w_n^* = 0$ for all $n \geq 1$. By performing a stability analysis near the fixed point, we find that this fixed point is stable for all $N > 4$, again as in the phononless case [26].

(4) *Other unstable fixed points*: In addition to the fixed points (with $\lambda^* = 0$) discussed in Sec. IV C, we find two new fixed points (with $\lambda^* \neq 0$). However, we find numerically that they are unstable.

In summary, adding a cubic-anisotropy term in the action changes the nature of the second-order transition for $N > 4$ from Wilson-Fisher to the cubic universality class. By contrast, for $N \leq 4$, the transition remains weakly first order, due to the coupling to phonons.

-
- [1] S. Sachdev, *Quantum Phase Transitions* (Cambridge University Press, Cambridge, 2011).
- [2] O. K. Rice, Thermodynamics of phase transitions in compressible solid lattices, *J. Chem. Phys.* **22**, 1535 (1954).
- [3] C. Domb, Specific heats of compressible lattices and the theory of melting, *J. Chem. Phys.* **25**, 783 (1956).
- [4] M. E. Fisher, Renormalization of critical exponents by hidden variables, *Phys. Rev.* **176**, 257 (1968).
- [5] A. I. Larkin and S. A. Pikin, Phase transitions of the first order but nearly of the second, *Zh. Eksp. Teor. Fiz.* **56**, 1664 (1969) [*Sov. Phys. JETP* **29**, 891 (1969)].
- [6] D. J. Bergman and B. I. Halperin, Critical behavior of an Ising model on a cubic compressible lattice, *Phys. Rev. B* **13**, 2145 (1976).
- [7] M. A. de Moura, T. C. Lubensky, Y. Imry, and A. Aharony, Coupling to anisotropic elastic media: Magnetic and liquid-crystal phase transitions, *Phys. Rev. B* **13**, 2176 (1976).
- [8] J. Bruno and J. Sak, Renormalization group for first-order phase transitions: Equation of state of the compressible Ising magnet, *Phys. Rev. B* **22**, 3302 (1980).
- [9] H. Wagner and J. Swift, Elasticity of a magnetic lattice near the magnetic critical point, *Z. Phys.* **239**, 182 (1970).
- [10] A. Aharony, Critical behavior of magnets with lattice coupling, *Phys. Rev. B* **8**, 4314 (1973).
- [11] F. J. Wegner, Magnetic phase transitions on elastic isotropic lattices, *J. Phys. C* **7**, 2109 (1974).
- [12] M. Sitte, A. Rosch, J. S. Meyer, K. A. Matveev, and M. Garst, Emergent Lorentz Symmetry with Vanishing Velocity in a Critical Two-Subband Quantum Wire, *Phys. Rev. Lett.* **102**, 176404 (2009).
- [13] L. Huijse, B. Bauer, and E. Berg, Emergent Supersymmetry at the Ising–Berezinskii–Kosterlitz–Thouless Multicritical Point, *Phys. Rev. Lett.* **114**, 090404 (2015).
- [14] O. Alberton, J. Ruhman, E. Berg, and E. Altman, Fate of the one-dimensional Ising quantum critical point coupled to a gapless boson, *Phys. Rev. B* **95**, 075132 (2017).
- [15] P. Chandra, P. Coleman, M. A. Continentino, and G. G. Lonzarich, Quantum annealed criticality: A scaling description, *Phys. Rev. Research* **2**, 043440 (2020).
- [16] S. E. Han, J. Lee, and E.-G. Moon, Lattice vibration as a knob on exotic quantum criticality, *Phys. Rev. B* **103**, 014435 (2021).

- [17] S. E. Rowley, L. J. Spalek, R. P. Smith, M. P. M. Dean, M. Itoh, J. F. Scott, G. G. Lonzarich, and S. S. Saxena, Ferroelectric quantum criticality, *Nat. Phys.* **10**, 367 (2014).
- [18] T. F. Nova, A. S. Disa, M. Fechner, and A. Cavalleri, Metastable ferroelectricity in optically strained SrTiO₃, *Science* **364**, 1075 (2019).
- [19] K. Ahadi, L. Galletti, Y. Li, S. Salmani-Rezaie, W. Wu, and S. Stemmer, Enhancing superconductivity in SrTiO₃ films with strain, *Sci. Adv.* **5**, eaaw0120 (2019).
- [20] U. Aseginolaza, R. Bianco, L. Monacelli, L. Paulatto, M. Calandra, F. Mauri, A. Bergara, and I. Errea, Phonon Collapse and Second-Order Phase Transition in Thermoelectric SnSe, *Phys. Rev. Lett.* **122**, 075901 (2019).
- [21] M. Brando, D. Belitz, F. M. Grosche, and T. R. Kirkpatrick, Metallic quantum ferromagnets, *Rev. Mod. Phys.* **88**, 025006 (2016).
- [22] W. C. Vieira and P. R. S. Carvalho, Robustness of the O(N) universality class, *Europhys. Lett.* **108**, 21001 (2014).
- [23] K. G. Wilson, Feynman-Graph Expansion for Critical Exponents, *Phys. Rev. Lett.* **28**, 548 (1972).
- [24] K. G. Wilson and M. E. Fisher, Critical Exponents in 3.99 Dimensions, *Phys. Rev. Lett.* **28**, 240 (1972).
- [25] K. G. Wilson and J. Kogut, The renormalization group and the ϵ expansion, *Phys. Rep.* **12**, 75 (1974).
- [26] A. Aharony, Critical behavior of anisotropic cubic systems, *Phys. Rev. B* **8**, 4270 (1973).
- [27] R. A. Cowley and A. D. Bruce, Application of the Wilson theory of critical phenomena to a structural phase transition, *J. Phys. C* **6**, L191 (1973).
- [28] T. Nattermann and S. Trimper, Critical behaviour and cubic anisotropy, *J. Phys. A* **8**, 2000 (1975).
- [29] D. J. Binder, The cubic fixed point at large N , *J. High Energy Phys.* **09** (2021) 071.
- [30] A. Aharony, O. Entin-Wohlman, and A. Kudlis, Different critical behaviors in perovskites with a structural phase transition from cubic-to-trigonal and cubic-to-tetragonal symmetry, *Phys. Rev. B* **105**, 104101 (2022).
- [31] Y.-C. Zhang, F. Maucher, and T. Pohl, Supersolidity around a Critical Point in Dipolar Bose-Einstein Condensates, *Phys. Rev. Lett.* **123**, 015301 (2019).
- [32] L. Pili and S. A. Grigera, Two-dimensional Ising model with Einstein site phonons, *Phys. Rev. B* **99**, 144421 (2019).
- [33] I. Shamai and D. Podolsky, Molten antiferromagnets in two dimensions, [arXiv:1801.08131](https://arxiv.org/abs/1801.08131).
- [34] D. Abutbul and D. Podolsky, Topological Order in an Antiferromagnetic Tetratic Phase, *Phys. Rev. Lett.* **128**, 255501 (2022).